ARTICLES

Journal of Semiconductors
(2023) 44, 032602
doi: 10.1088/1674-4926/44/3/032602

Self-healing Au/PVDF-HFP composite ionic gel for flexible underwater pressure sensor

Ruiyang Yin[1, 3], Linlin Li[1, 2], Lili Wang[1, 2], and Zheng Lou[1, 2, †]

[1]State Key Laboratory for Superlattices and Microstructures, Institute of Semiconductors, Chinese Academy of Sciences, Beijing 100083, China
[2]Center of Materials Science and Optoelectronic Engineering, University of Chinese Academy of Sciences, Beijing 100083, China
[3]Department of Materials Science and Engineering, College of Engineering, Peking University, Beijing 100871, China

Abstract: Ionic gels can be potentially used in wearable devices owing to their high humidity resistance and non-volatility. However, the applicability of existing ionic gel pressure sensors is limited by their low sensitivity. Therefore, it is very important to develop an ionic gel pressure sensor with high sensitivity and a wide pressure detection range without sacrificing mechanical stretchability and self-healing ability. Herein, we report an effective strategy for developing pressure sensors based on ionic gel composites consisting of high-molecular-weight polymers, ionic liquids, and Au nanoparticles. The resulting capacitive pressure sensors exhibit high pressure sensitivity, fast response, and excellent self-healing properties. The sensors composed of highly hydrophobic polymers and ionic liquids can be used to track underwater movements, demonstrating broad application prospects in human motion state monitoring and underwater mechanical operations.

Key words: ionic gel; pressure sensor; high performance; underwater operation; self-healing

Citation: R Y Yin, L L Li, L L Wang, and Z Lou, Self-healing Au/PVDF-HFP composite ionic gel for flexible underwater pressure sensor[J]. *J. Semicond.*, 2023, 44(3), 032602. https://doi.org/10.1088/1674-4926/44/3/032602

1. Introduction

Conductive gel materials have attracted significant attention in the fields of wearable devices, implantable biosensors, and artificial intelligence[1–12] owing to their high conductivity, flexibility, and biocompatibility[13–19]. Among the gel materials, hydrogel materials are widely concerned and studied. However, they usually rely on hydrophilic polymer chains and hydrogen bonds[20–24]. High humid or temperature environments may reduce the performance of such materials, and the volatilization of hydrogel materials in the open air will influence their long-term stability, which has a negative impact on its application scenario and lifetime[25–30].

Ionic gel is a material consisting of a polymer as a network structure with ionic liquid instead of water filled in it[29, 31, 39]. Their unique advantages, such as non-volatility, high thermal stability, and high electrochemical stability, enable the replacement of hydrogel materials with ionic gels in various applications[22, 23, 32]. In recent years, various strategies have been developed to improve the properties of ionic gels, including self-healing ability, flexibility, extensibility, water resistance, and self-adhesiveness[33–35]. For example, Wang *et al.*[29] obtained a high-strength stretchable ionic gel by randomly copolymerizing two common monomers with different solubilities in ionic liquids to generate phase-separated elastic and rigid domains in situ. Li *et al.*[36] prepared an extremely durable ionic skin with excellent self-healing performance and high sensitivity by immersing an ionic liquid into a polyurethane network with good mechanical properties. Although the above-mentioned research studies have considerably improved the toughness and self-healing properties of ionic gel materials[23, 24, 37], their conductivity was not significantly increased, which limited their scalability. Wearable sensors based on ionic gels are limited owing to the low sensitivity and slow response. The incorporation of conductive particles into ionic gel materials is an effective method to address these issues[38–41].

In this study, we propose a flexible, submersible, and self-healing pressure sensor based on a novel Au nanoparticle ionic gel composite material. We have selected poly(vinylidene fluoride-co-hexafluoropropylene) (PVDF-co-HFP) as a polar polymer network and (1-ethyl-3-methylimidazolium bis(trifluoromethylsulfonyl)imide) (EMI–TFSI) as an ionic liquid to create highly reversible ion–dipole interactions, which endow the ionic gel with high flexibility and self-healing properties at room temperature[33, 35, 42]. A novel in situ vapor deposition composite method was applied to introduce Au nanoparticles into the gel structure, which is found to be an effective large-scale production method[43, 44]. The ionic gel sensor based on the prepared Au nanoparticle composite operated according to a new capacitive pressure sensing mechanism. In addition, owing to the use of highly hydrophobic polymers and ionic liquids, the sensor fabricated from the ionic gel was not affected by external humidity even during the regular underwater operation. The produced pressure sensor was utilized to measure different water depths, perceive a robot grasping objects underwater, and monitor the underwater movement of a submarine toy in real time.

2. Methods

2.1. Synthesis process of ionic gel

The fabrication progress is shown in the Fig. 1(c) in de-

Correspondence to: Z Lou, zlou@semi.ac.cn
Received 4 NOVEMBER 2022; Revised 13 DECEMBER 2022.
©2023 Chinese Institute of Electronics

tail. First, 1 g PVDF-co-HFP-5545 (3M Dyneon Fluoroelastomer FE) and 0.35 g EMITFSI were dissolved in 4.5 mL N, N-dimethylformamide (DMF). The mixture was stirred for at least 4 h at room temperature until a transparent and well-dispersed solution was obtained. The solution was placed in the refrigerator for 12 h to remove bubbles and then the solution was poured into a Petri dish to dry the DMF solvent at 60 ℃ in a vacuum oven. Afterwards, Au nanoparticles were composited into ionic gels via evaporation method. The size and composite concentration of Au nanoparticles were largely determined by the evaporation rate and thickness, thus affecting the electrical properties and pressure sensing properties of the ionic gels. Then 10 g film was re-dissolved by 50 mL DMF solvent and once again the film was dried in the oven to obtain the sample sheet.

2.2. Mechanical properties

The tensile and compressive pressure tests of the ionic gel material are tested at room temperature using the Instron fatigue tensile machine. In the tensile test, the shape of the sample is a rectangular parallelepiped with a thickness of about 2 mm, a length of about 20 mm and a width of about 10 mm, and the tensile rate is fixed at 10 mm/min. The stress is calculated by $\sigma = F/A_0$, where F is the applied force and A_0 is the contact area at the beginning.

2.3. Characterization method

All ionic gel materials were cut into thin films with a thickness of approximately 1 mm for characterization testing. Ultraviolet absorption spectrum test is tested by UV-3600 ultraviolet-visible-near-infrared spectrophotometer, the test range of absorption spectrum is in the visible range; infrared absorption spectrum test is determined by Nicolet IS10 infrared spectrometer, the measurement range is 500–4000 cm^{-1}; Raman spectrum test is measured by a Renishaw in Via Raman spectrometer, the excitation wavelength is 532 nm, and the scanning range is 100–2000 cm^{-1}.

2.4. Determination of pressure capacity type pressure performance

The compression resistance pressure sensing performance of the ionic gel material is measured using an impedance analyzer and an Instron fatigue tensile machine. In the pressure test, the sample was cut into a rectangular parallelepiped with a thickness of about 2 mm and a length of about 10 cm. Cu electrodes were attached to the upper and lower surfaces of the ion gel to form a parallel plate capacitor. The selected working voltage of the impedance analyzer is 1 V, the working frequency is 10 kHz, and the fatigue tensile testing machine gradually changes from load 0.1 to 5 N. The pressure of the sample is calculated by $P = F/S$, where F is the pressure applied on the surface of the sensor, and S is the force area of the sensor.

3. Results and discussion

The performance of a gel material is strongly related to its constitution. The ionic gel fabricated in this study consists of three main components: a highly polar fluoro-elastomer, poly (vinylidene fluride-hexafluoropropylene) (PVDF-HFP-5545); fluorine-rich ionic liquid EMI–TFSI, and Au nanoparticles (Fig. 1(a)). The polymer network PVDF-co-HFP-5545 combines the highly crystalline PVDF with highly polar HFP. Owing to the ion–dipole interactions between polymer chains and the ionic liquid, the ionic gel exhibits good self-healing properties at room temperature. Moreover, because C–F (carbon–fluorine) bonds are weak hydrogen donors and acceptors, fluorine-rich ionic gels are rarely affected by water molecules and can operate in wet and even underwater environments, which represents a major advantage of ionic gel materials over the commonly used hydrogen bond-based hydrogels[14, 33]. Au nanoparticles are evenly distributed in the gel via an evaporation deposition route. The uniform doping of Au nanoparticles is attributed to various factors, such as the high temperature of the evaporation process, ionic gel modification effect, and real-time self-healing properties of the gel at high temperatures.

The addition of Au nanoparticles not only preserves the good self-healing and tensile properties of the ionic gel but also changes its electrical properties by increasing the conductive path in the ionic gel structure. This increases the probability of charge transfer after the application of an external voltage, which allows the use of gel materials as functional sensors and flexible electronic devices[24, 39] (Fig. 1(b)). Specifically, we attribute the ionic gel self-healing properties to the existence of reversible ionic interactions at room temperature. Furthermore, the mechanism of pressure sensing can be explained by the increase in the charge storage capacity caused by Au nanoparticle addition, which is discussed in more detail in the subsequent sections (Fig. 1(c)).

We propose a new method for the large-area doping of Au nanoparticles into gels[14–23, 37]. Fig. 1(d) illustrates the ionic gel fabrication process. First, PVDF-co-HFP-5545 and EMI–TFSI were dissolved in dimethylformamide (DMF) and stirred thoroughly until a transparent and well-dispersed solution was obtained. This solution was dried in a vacuum oven to produce a flat gel film, after which gold nanoparticles were introduced into the gel structure through an evaporation method. Finally, the ionic gel membrane was re-dissolved in DMF and dried again to obtain a gel sample. A photograph of the obtained ionic gel is presented in Supplementary Fig. S1. It shows that the ionic gel is highly transparent and contains Au nanoparticles with the unique faint wine red color. Using this method, ionic gel membranes can be easily prepared on a large scale. In addition, we synthesized other metal nanoparticles, such as Cu, Ni, Ag, and Cr, with different colors (Fig. S2). Compared with traditional nanoparticle fabrication methods (such as citric acid reduction), the technique utilized in this study is simpler and less expensive while enabling large-area nanoparticle compositing. The particle size and vapor deposition distribution density strongly depend on vaporization rate and thickness. In fact, various evaporation conditions result in ionic gel films with different colors owing to the different size and density of metal particles, which strongly affects the ionic gel sensing performance. Therefore, to maintain consistency of the utilized gel material, the same evaporation conditions were used to fabricate the functional layer of the capacitive pressure sensor and preserve its good self-healing and underwater operational characteristics.

We utilized various characterization methods to analyze the morphology and composition of the synthesized ionic gel material. Fig. 2(a) displays typical scanning electron microscopy (SEM) images of the ionic gel. They show that its basic structure is composed of PVDF–HFP polymer. The ionic li-

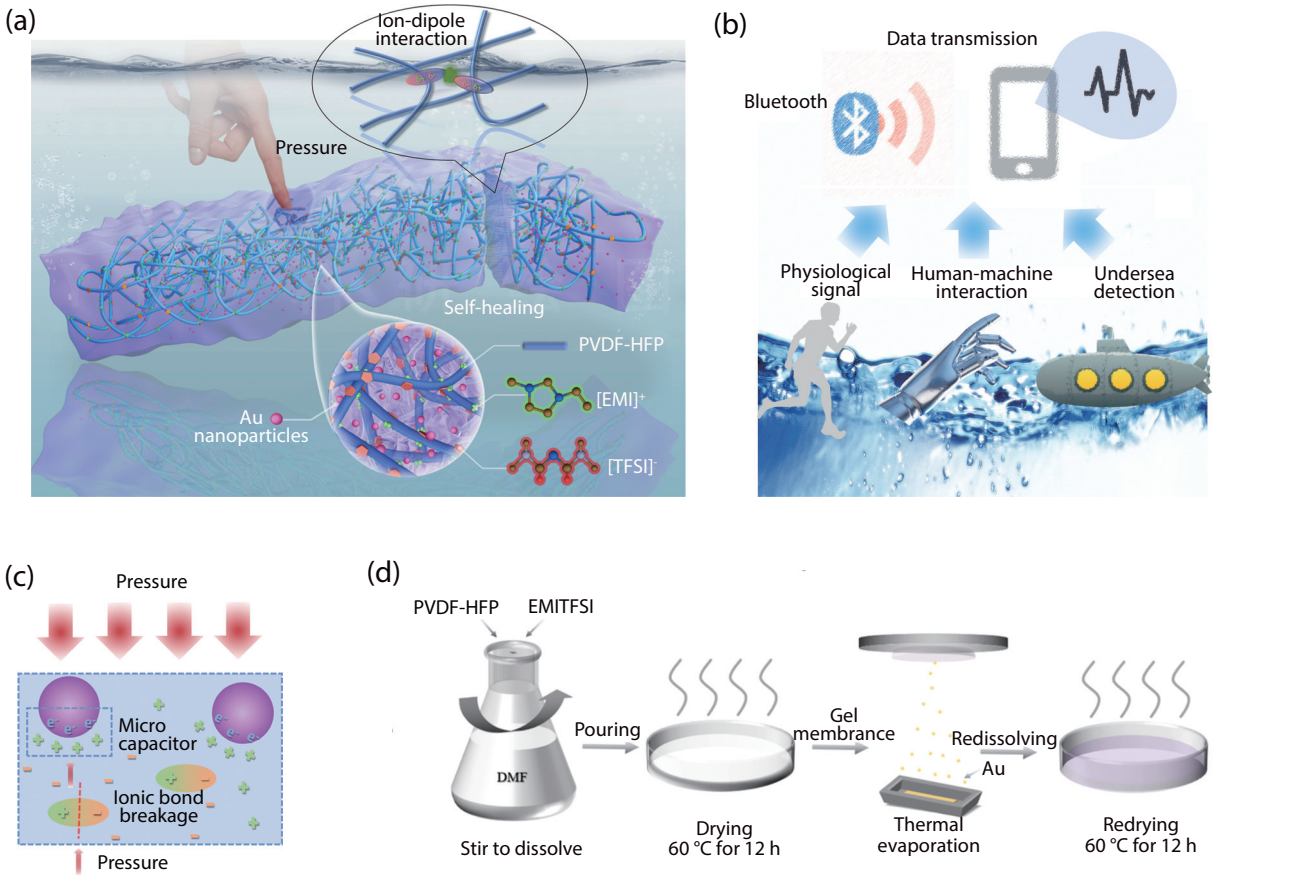

Fig. 1. (Color online) Design and fabrication of transparent, mechanically robust, and ultrastable ionic gels enabled by ionic interactions. (a) Schematic diagram of ionic gel design. (b) Potential applications of ionic gel in different fields. (c) Self-healing and sensing mechanism of ionic gel materials. (d) Schematic diagram of ionic gel synthesis process.

quid is coupled with the polymer network through ionic interactions, and Au nanoparticles are wrapped into polymer chains, thereby effectively inhibiting the agglomeration of Au nanoparticles. Fig. 2(b) presents the elemental mapping images of the ionic gel. It shows that the representative elements N, S, and Au are uniformly distributed in the material structure. Among these elements, N and S are the characteristic elements of EMI^+ cations and $TFSI^-$ anions. The transmission electron microscopy (TEM) image depicted in Fig. S3 displays the Au nanoparticles with sizes of tens of nanometers. Owing to the interactions between the ionic gel and ions, the produced film exhibits distinct hydrophobic characteristics (Supplementary Fig. S4; note that the ionic gel contact angle is approximately 110°).

The ultraviolet absorption spectra recorded before and after the introduction of Au nanoparticles are shown in Fig. 2(c). After Au incorporation, the absorption peak intensity at 530 nm is significantly enhanced. According to the formula $y = 0.786x + 503.53$, where y and x represent the intensity of the ultraviolet absorption peak and diameter of Au nanoparticles, respectively, the size of Au nanoparticles is approximately 30–40 nm. Its magnitude depends on various factors, such as the current used during vapor deposition, vapor deposition rate, and ion gel film thickness. The same parameters were consistently utilized during the introduction of Au nanoparticles to achieve the same doping effect.

The infrared absorption spectra presented in Fig. 2(d) show that the polymer covalent bonds of the ionic gel were not destroyed after the incorporation of Au nanoparticles. Therefore, the polymer skeleton inside the ionic gel composed of basic covalent bonds remained unchanged. Figs. 2(e) and 2(f) display the Raman absorption spectra of the ionic gel obtained in the ranges of 2900–3000 and 730–760 cm^{-1}, corresponding to the characteristic absorption peaks of EMI^+ vibrational bands and the $TFSI^-$ expansion contraction mode respectively. By characterizing the nanogel morphology and composition, we confirmed the chemical components and their distribution in the ionic gel composite.

The mechanical properties of the ionic gel, including high strain failure points, Young's modulus, and maximum tensile stress, are presented in Figs. 2(g) and S5. The composite mechanical properties did not significantly change after incorporating Au nanoparticles. Owing to the ionic dipole moment interactions between the C–F bonds of PVDF–HFP and ionic liquid, the ionic gel retained good self-healing characteristics even at room temperature. A photograph of the self-healing process is presented in Fig. 2(h). In this experiment, the gel was cut with a knife, and the produced scratch gradually disappeared after room temperature storage. Similarly, we cut the gel with a blade and placed the two pieces attached to each other into water at room temperature. After some time, the two gel pieces naturally bonded, and the scratches gradually disappeared, as shown in the optical microscopy images obtained at certain intervals (Fig. S6). The self-healing process examined from another angle is illustrated by the SEM images obtained before and after self-healing (Fig. S7). During the self-healing process, polymer skeletons approach each other under the action of the ionic dipole moment and ulti-

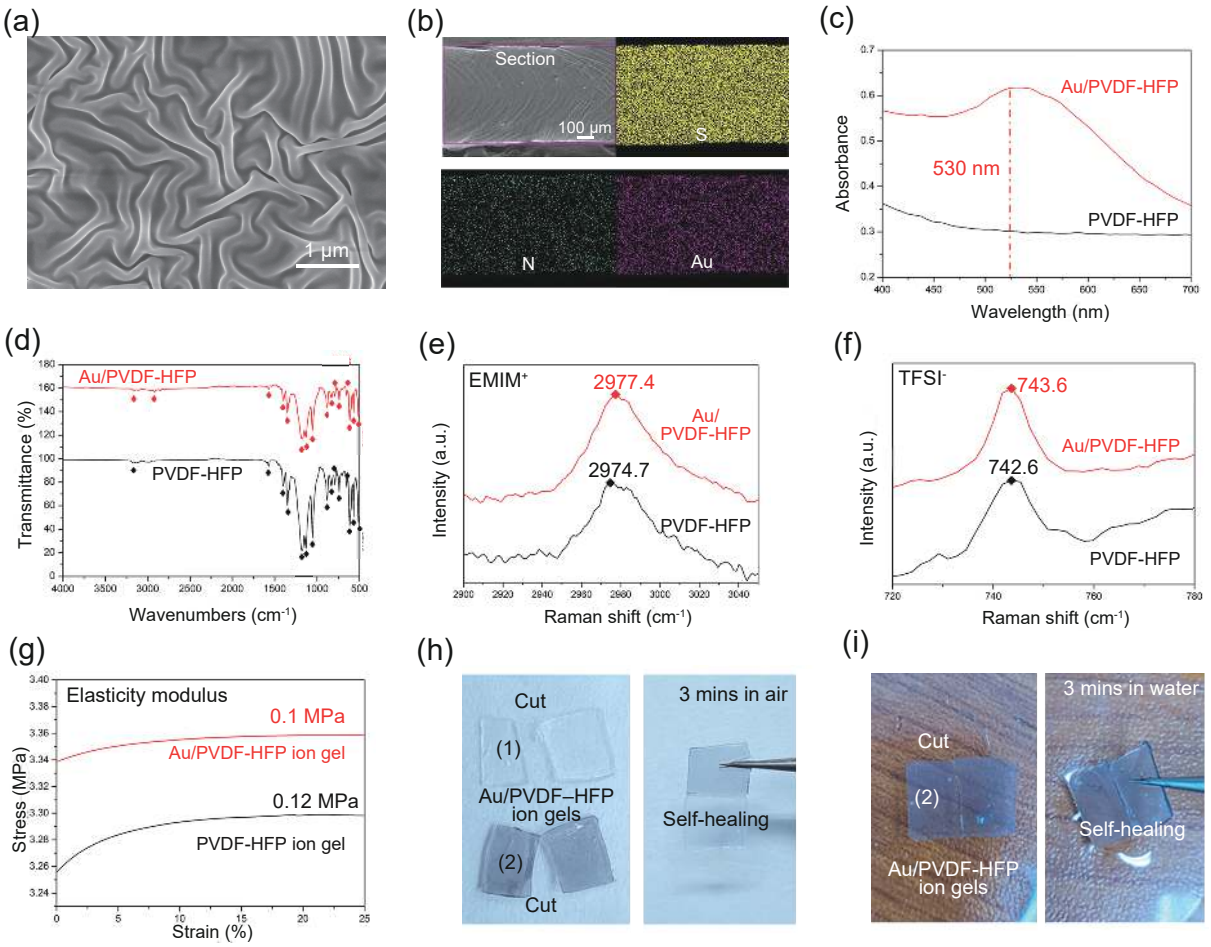

Fig. 2. (Color online) Morphology and characterization of ionic gel. (a) Schematic diagram of ionic gel SEM. (b) Element analysis of gel section slices, respectively showing the uniform distribution of S, N, and Au. (c) UV absorption spectra of ionic gels before and after doping Au nanoparticles. After doping with Au nanoparticles, an obvious peak appears in the band around 530 nm. (d) Comparison of infrared absorption spectra before and after doping Au nanoparticles. There was no change in the covalent bond before and after the Au nanoparticles were recombined. (e, f) Raman spectra before and after doping Au nanoparticles. The Raman spectra in the spectral range 720–780 cm^{-1} corresponding to $EMIM^+$ vibrational bands. The Raman peak in the range of 720–780 cm^{-1} corresponding to $TFSI^-$ anion expansion–contraction mode. (g) Mechanical tensile properties and Young's modulus. The self-healing process of the physical image: (h) The picture above shows self-healing naturally at room temperature for 3 min, and (i) the picture below shows self-healing under water.

mately become restacked and crosslinked. The current and capacitance changes measured before and after self-healing are presented in Figs. S8 and S9 respectively. They show that within a few tens of seconds, the current and capacitance of the ionic gel recovered to the levels measured before self-healing. These results confirm that the ionic gel material can rapidly self-heal at room temperature without changing its electrical properties.

Cu electrodes were attached to the upper and lower surfaces of the ionic gel to form a parallel plate capacitor (Fig. 3(a)). When an external pressure was applied to the device, its capacitance increased, as indicated by impedance analyzer readings. Next, we constructed an ionic gel model to elucidate the capacity pressure sensing mechanism (Fig. 3(b)). Without an external force, Au nanoparticles and the EMI–TFSI ionic liquid are disorderly distributed inside the gel. Macroscopically, the capacitance C is defined by the formula $C = Q/U = \varepsilon S/4\pi kd$. According to this definition, the applied external force initiates a charge movement and increases the probability of charge transport by Au nanoparticles. Therefore, the externally applied pressure affects the dielectric constant ε of the ionic gel. As a result, the charge between the two parallel plates is changed, causing capacitance variations with the external pressure. From a microscopic perspective, the externally applied pressure produced two effects: (1) the external force partially disrupted the ionic interactions between EMI^+ and $TFSI^-$ ions, and (2) the gel components were brought closer together. Under the applied voltage conditions, free electrons are generated on the surface of Au nanoparticles, and the positive and negative ions separated by the external force are easily captured by Au nanoparticles to form miniature capacitors, which significantly enhance the charge storage ability of the dielectric layer. Therefore, the external force can effectively increase the capacitance of the device, which allows its use as a capacitive pressure sensor.

Because the capacitive pressure sensitivity of the device is significantly affected by frequency, we measured capacitance changes at different test frequencies (Fig. 3(c)). As the test frequency increased, the device capacitance gradually decreased and stabilized in the high-frequency range. Therefore, all the subsequent pressure tests were performed at a test frequency of 10 kHz with a stable capacitance. First, we recorded the capacitance change versus frequency curves at

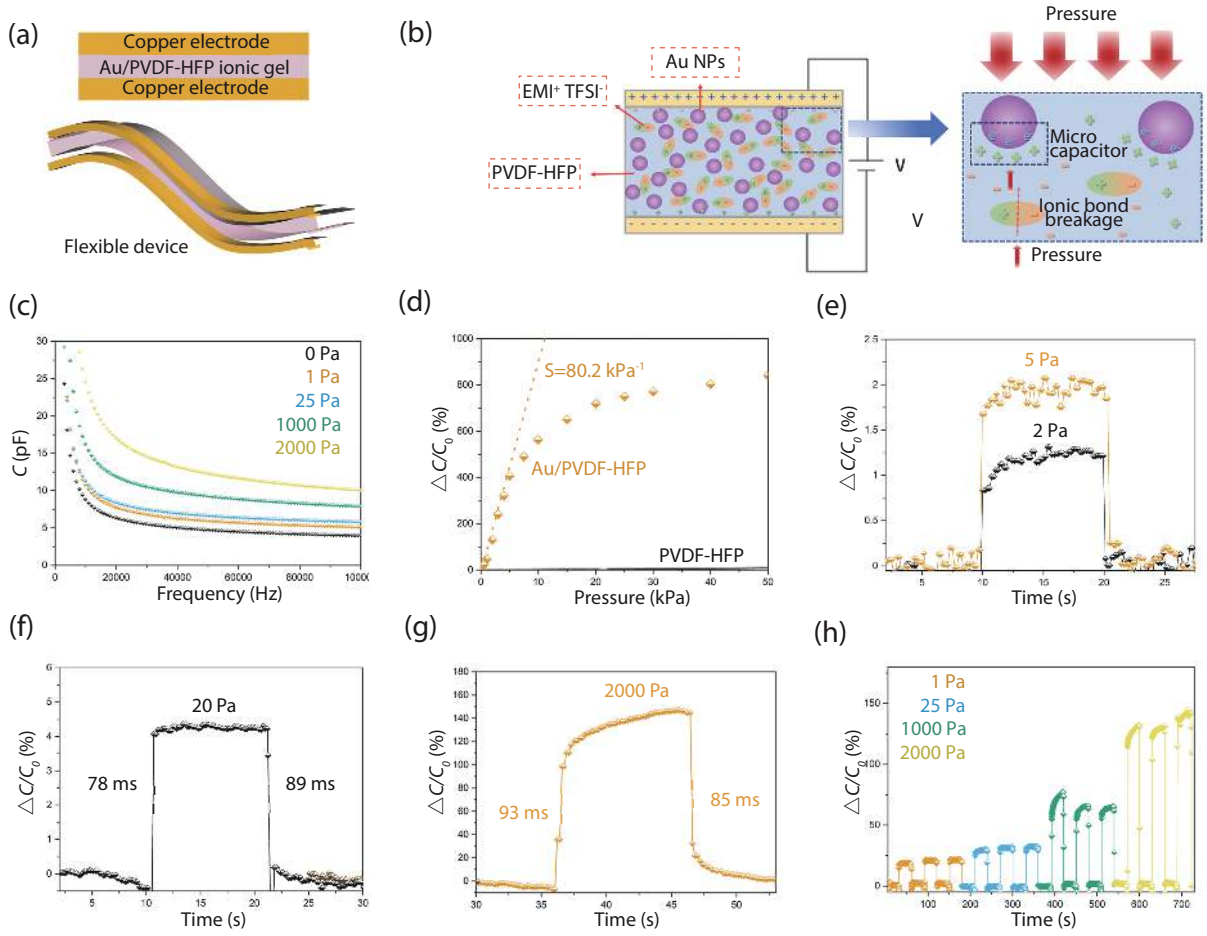

Fig. 3. (Color online) Pressure sensor performance. (a) Schematic diagram of the structure for capacitive pressure sensor device. (b) Principle model of pressure sensor. (c) Frequency sweep of capacitive pressure sensor under different pressures. (d) Sensitivity curve of capacitive pressure sensor. (e) Perception of slight pressure. (f, g) Response/recovery speed under 20 Pa and 2 kPa pressure. (h) Continuous testing of different pressures.

different pressures, which showed that at the same frequency, the capacitance was larger when applying larger pressure. Next, typical pressure sensitivity tests were conducted. Fig. 3(d) displays the pressure sensitivity curve of the capacitive pressure sensor with relatively high pressure values. The sensitivity of a capacitive-type pressure sensor is defined as $S = \delta(\Delta C/C_0)/\delta P$, where C and C_0 represent the measured capacitance and initial capacitance before pressure application, respectively. In the pressure range below 10 kPa, the sensitivity of the capacitive pressure sensor was approximately 0.8 k/Pa. Compared with pure ionic gels, the sensitivity of the sensor containing composite Au nanoparticles was higher by two orders of magnitude. Even in the high-pressure range (above 10 kPa), the pressure sensor maintained the high sensitivity. Fig. 3(e) shows that the pressure sensor exhibits a strong response to a small pressure, such as 2 and 5 Pa. Moreover, 2 and 5 Pa pressure can be clearly distinguished, indicating its broad detection range and discrimination. Meanwhile, the capacitive pressure sensor also demonstrated high response speed. After applying both a small pressure of 20 Pa or large pressure of 2 kPa, the sensor rapidly responded within 100 ms (Figs. 3(e) and 3(g)). Fig. 3(h) further indicates that the sensor exhibits high continuous operating stability and distinguishability under various pressure conditions.

To confirm the feasibility of the large-area vapor deposition of composite Au nanoparticles, the ionic gel fabricated via the vapor deposition method was compared with the ionic gel obtained by physically mixing Au nanoparticles synthesized through the direct citric acid reduction in the gel. Evaluating the pressure-sensing devices fabricated from both gels, their properties were very similar, indicating that the vapor deposition of Au nanoparticles was a feasible preparation method (Fig. S10). The influences of evaporation rate and evaporation thickness on the pressure sensing performance discussed above are illustrated in Fig. S11. At the same external pressure, the higher the evaporation thickness and evaporation rate, the larger the sensor capacitance change and higher the pressure sensitivity. To verify that evaporating metal nanoparticles into the ionic gel was a universal and effective preparation method, we fabricated capacitive pressure sensors by vaporizing other metal nanoparticles. For example, Fig. S12 describes the performance of the pressure sensor composed of Ag nanoparticles, which confirms the universality of the vapor deposition method for manufacturing pressure sensors from metal nanoparticles and ionic gels.

We used the ionic gel as a capacitive pressure sensor accomplishing high sensitivity and stable performance. In addition, the prepared gel demonstrated high application potential in sensing other parameters. Fig. S13 illustrates its use as a resistive pressure sensor (with a structure identical to that of the pressure sensor containing Au nanoparticles). After applying a pressure of 2 kPa, the sensor resistance increased by

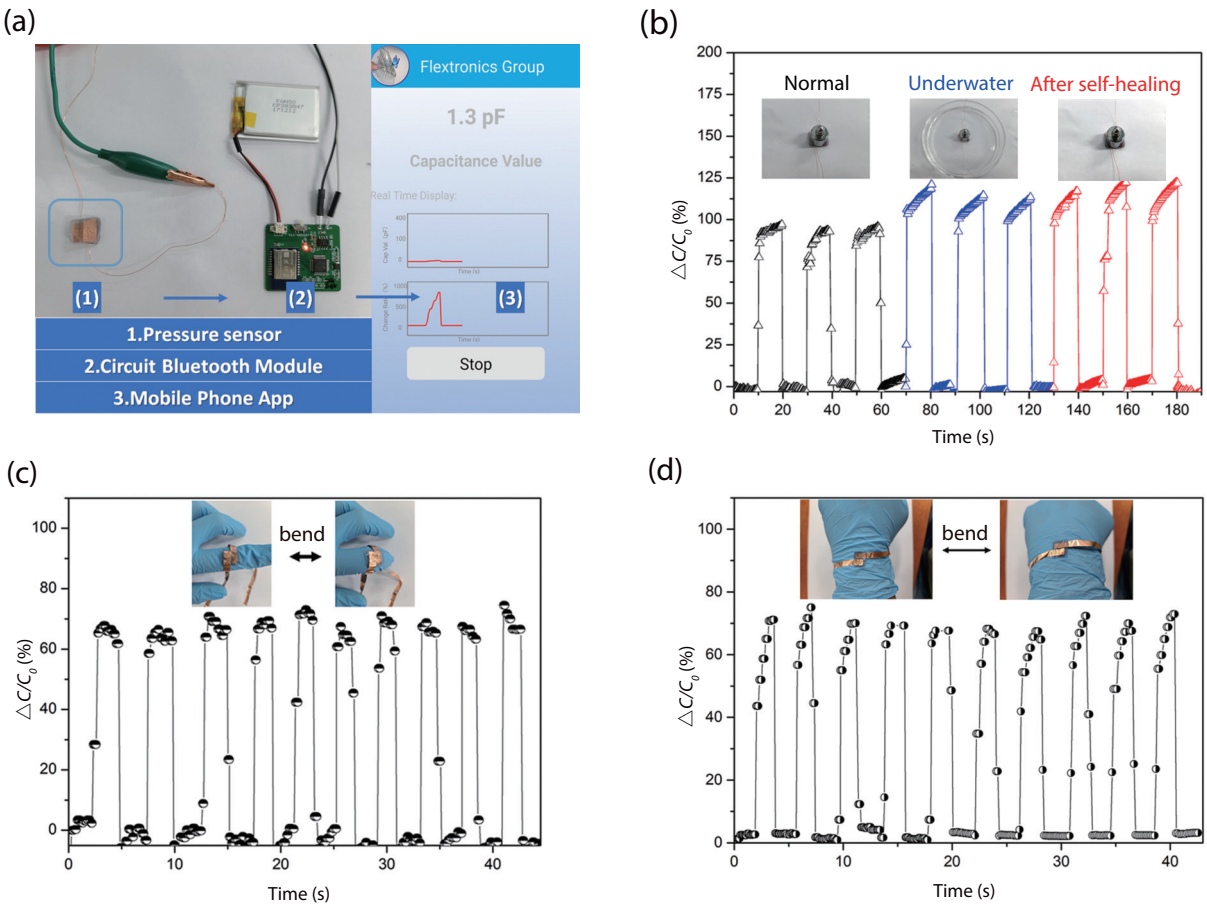

Fig. 4. (Color online) Simple application in life. (a) Schematic diagram of the device used for underwater testing. (b) 2 kPa pressure perception under three different conditions (normal, underwater and after self-healing). (c) Finger bending perception. (d) Arm movement perception.

more than an order of magnitude. As discussed above, the addition of Au nanoparticles increases the probability of charge transport as compared with that of the pure ionic gel, thereby changing the current passing through the device (Fig. S14). Furthermore, Fig. S15 suggests that the device possesses good non-contact characteristics. As a human finger gradually approached the device from a certain distance, its capacitance gradually decreased unlike the increase in capacitance observed after increasing the external pressure. This phenomenon might be due to the electrostatic polarization of the ionic gel caused by the close proximity to the human skin and other charged objects, which was assisted by Au nanoparticles, confirming the applicability of the gel material as a non-contact device after further optimization. The obtained results demonstrate the high potential of the produced ionic gel for multi-field sensing and multi-functional integration.

By employing the fabricated capacitive pressure sensor, we performed some daily-life experiments and further demonstrated the unique characteristics of the new ionic gel material, rendering it suitable for underwater applications. We used the circuit design depicted in Fig. 4(a) to transfer pressure signal changes of the device operating underwater to a mobile application. The utilized circuit system was divided into three parts: a pressure sensor, Bluetooth module, and mobile phone application. The capacitive pressure sensor was encapsulated by the same ionic gel material without adding Au nanoparticles to maintain its self-healing properties.

Owing to the high adhesion and good self-healing characteristics of the ion gel material, the internal pressure sensor was tightly sealed. Because the polymer chains in the ionic gel structure mainly consisted of C–F bonds, it was weakly affected by the hydrogen atoms of water molecules; therefore, the sensor could normally function and even self-heal in underwater environments. The Bluetooth circuit module outputs a certain frequency of alternating current to the sealed pressure sensor through Cu conductors coated with insulated enameled wires. Meanwhile, capacitance changes of the pressure sensor were detected by attaching Cu wires to the Bluetooth module for analysis and processing and were finally displayed on the mobile phone application. This design was employed for all the subsequent demonstrations.

After adopting this system, we first applied the same pressure of 2 kPa to the pressure sensor under three different conditions (normal operation, underwater, and after self-healing) to verify that the sensor maintained similar pressure sensitivities (Fig. 4(b)). No apparent capacitance variations were observed between the three cases, suggesting that the proposed sensor could be used for pressure measurements under different conditions. Similar to traditional pressure sensors, we attached the device to the human body to detect changes in its motion state. Figs. 4(c) and 4(d) show the schematics of the capacitance changes measured during sensing the movements of a human finger and wrist, respectively. When the human finger or wrist was bent or moved, a certain stress was generated in the pressure sensor structure, which changed the device capacitance. The obtained results revealed that when the finger and wrist were continuously bent at the same angle, the capacitance values presented in

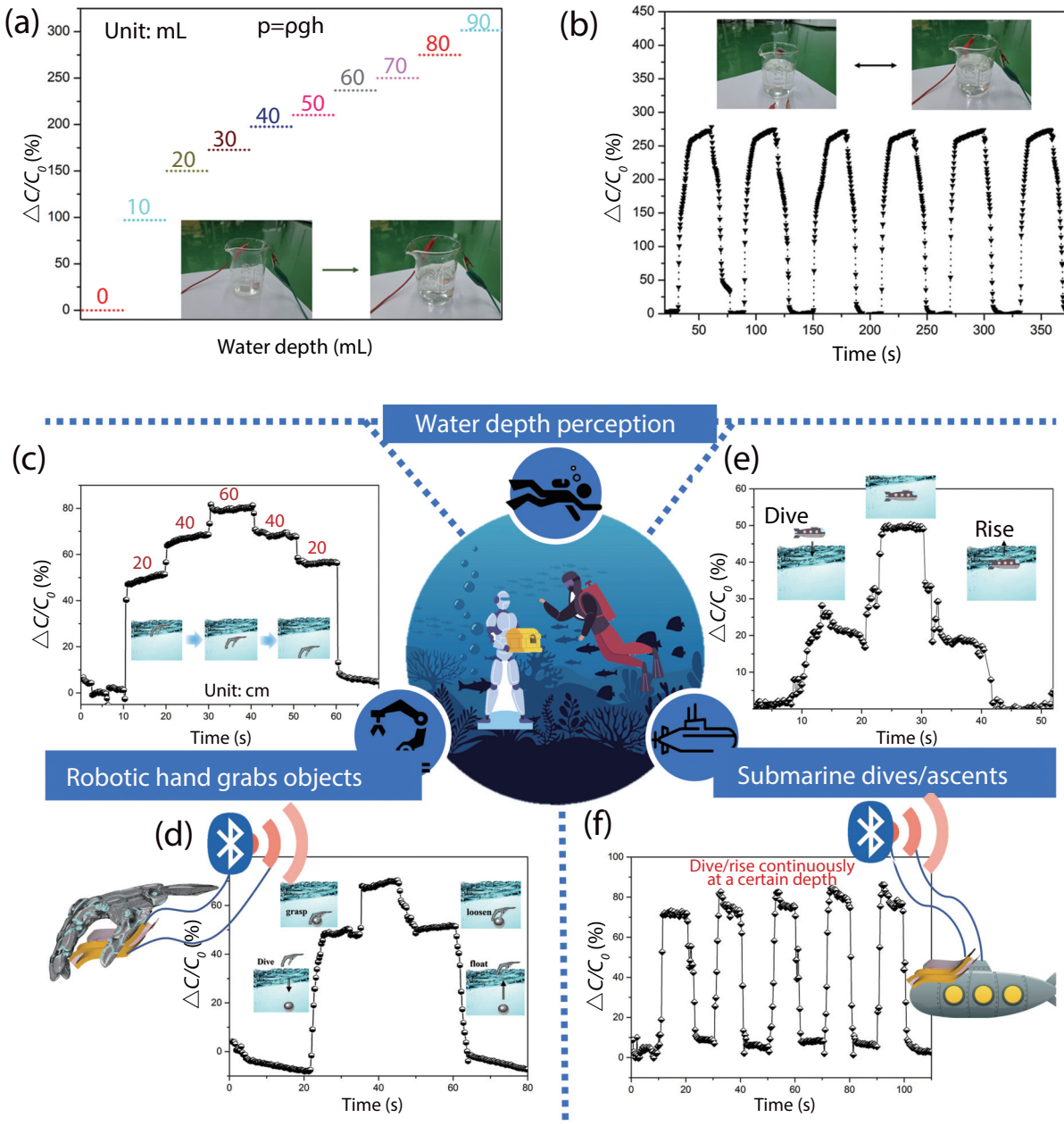

Fig. 5. (Color online) Practical underwater display. Perception of different water depths according to different water pressures. (a) Water depth measurement according to the proportional relationship between water pressure and water depth. (b) Continuous testing at the same water depth. Submarine diving and ascent process underwater (The sensor is attached to the palm of the robotic claw). (c) The sensor capacitance changes during the diving and ascent of the submarine. (d) The sensor capacitance changes when the submarine continuously dives/floats to a certain depth. Manipulator grabbing objects underwater (the sensor is attached to the head of submarine toy). (e) The capacitance of the pressure sensor changes when the mechanical gripper stays in different water depths. (f) The capacitance of the pressure sensor changes when the mechanical claw grabs an object underwater.

Figs. 4(c) and 4(d) changed accordingly. This property can be potentially used to monitor the respiration, pulse, and human motion status in future studies.

In general, pressure sensors that can be employed to measure the underwater pressure and water depth and exhibit good self-healing properties have broad application prospects in the fields of human motion state monitoring, underwater mechanical operations, and artificial intelligence. To verify the applicability of the fabricated pressure sensor in these fields, we conducted two practical demonstrations. First, the sensor was utilized to monitor the state of human movement underwater. At the same time, it was also employed for water depth testing. According to the formula $P = \rho gh$ (where P, ρ, and h represent the water pressure, liquid density, and water depth, respectively), the water pressure is proportional to the water depth. Based on this relationship, we measured the water depth in the beaker on the volume scale from 0 to 90 mL (Fig. 5(a)). Different water pressures produced different capacitance values, which confirmed the feasibility of using the sensor for underwater applications. Fig. 5(b) describes the reproducibility of the water depth pressure measurement results. The measured capacitance changes after repeatedly pouring the same amount of deionized water were maintained at approximately the same maximum values in the successive experiments, which indicated that the fabricated device exhibited high stability during con-

tinuous underwater testing.

Utilizing a mechanical manipulator to grab objects underwater to simulate mechanical operations that might be performed during industrial production and in real life (Fig. 5). For this purpose, we attached the fabricated gel device to the gripper of the manipulator and allowed the manipulator to go underwater and grab an object. As the mechanical gripper entered the water and gradually descended, the real-time capacitance displayed on the mobile phone application increased owing to the increased water pressure. Fig. 5(c) shows the capacitance changes observed during the gradual descending and ascending of the manipulator. The manipulator remained at water depths of 20, 40, and 60 cm for certain periods, and the measured capacitance values were consistent with the device positions. Furthermore, we ordered the manipulator to grab an iron ball in the water while monitoring capacitance changes (Fig. 5(d)). In this scenario, the manipulator first dived to the object depth. After grabbing the object underwater and holding it for a short period, the manipulator released the object and floated to the surface. This entire process confirms that by measuring capacitance changes, the manipulator operating state can be monitored underwater in real time.

In the second experiment, the movements of a submarine toy diving underwater were examined. For this purpose, we attached the ionic gel sensor to the surface of the submarine's head and then monitored the submarine state by measuring changes in the ionic gel capacitance. As shown in Fig. 5(e), the sensor capacitance increased when the submarine was placed on the water surface. The submarine gradually descended and remained at a fixed depth for some time, after which it rose to the surface. As discussed earlier, the submarine depth can be determined from the capacitance value displayed on the mobile phone application. After the submarine floated, the sensor capacitance returned to its original value (Fig. 5(f)). These results confirmed that the ionic gel pressure sensor successfully operated underwater and was able to monitor the motion state of the submarine.

4. Conclusion

To overcome the shortcomings of traditional pressure sensors and the currently used flexible wearable devices, we examined the properties of skin-like ionic gel materials and innovatively incorporated metal nanoparticles into ionic gels through metal vapor deposition. As a result, a pressure sensor with high flexibility, stretchability, conductivity, and self-healing performance was successfully constructed. This sensor exhibited a high pressure sensitivity of 0.8 k/Pa with a novel operational mechanism. It also demonstrated good self-healing performance, which allows its potential applications in various complex environments, including underwater operations.

Acknowledgements

This work was supported by the National Natural Science Foundation of China (NSFC, Grant Nos. 61874111, 62174152 and 62022079), the National Key Research and Development Program of China (Grant No. 2020YFB1506400), the Youth Innovation Promotion Association of the Chinese Academy of Sciences (No. 2020115), and the Strategic Priority Research Program of the Chinese Academy of Sciences (XDA16021200).

Appendix A. Supplementary materials

Supplementary materials to this article can be found online at https://doi.org/10.1088/1674-4926/44/3/032602.

References

[1] Rogers J A, Someya T, Huang Y G. Materials and mechanics for stretchable electronics. Science, 2010, 327, 1603
[2] Wang D Y, Wang L L, Shen G Z. Nanofiber/nanowires-based flexible and stretchable sensors. J Semicond, 2020, 41, 041605
[3] Darabi M A, Khosrozadeh A, Mbeleck R, et al. Skin-inspired multifunctional autonomic-intrinsic conductive self-healing hydrogels with pressure sensitivity, stretchability, and 3D printability. Adv Mater, 2017, 29, 1700533
[4] Li L L, Zhao S F, Ran W H, et al. Dual sensing signal decoupling based on tellurium anisotropy for vr interaction and neuro-reflex system application. Nat Commun, 2022, 13, 5975
[5] Zhao S F, Ran W H, Lou Z, et al. Neuromorphic-computing-based adaptive learning using ion dynamics in flexible energy storage devices. Natl Sci Rev, 2022, 9, nwac158
[6] Mak P I. Lab-on-COS-an in-vitro diagnostic (IVD) tool for a healthier society. J Semicond, 2020, 41, 110301
[7] Das C M, Kang L, Ouyang Q Y, et al. Advanced low-dimensional carbon materials for flexible devices. InfoMat, 2020, 2, 698
[8] Park J, Hwang J C, Kim G G, et al. Flexible electronics based on one-dimensional and two-dimensional hybrid nanomaterials. InfoMat, 2020, 2, 33
[9] Jiang H, Zheng L, Liu Z, et al. Two-dimensional materials: From mechanical properties to flexible mechanical sensors. InfoMat, 2020, 2, 1077
[10] Hou Y X, Wang L, Sun R, et al. Crack-across-pore enabled high-performance flexible pressure sensors for deep neural network enhanced sensing and human action recognition. ACS Nano, 2022, 16, 8358
[11] Jia M, Yi C, Han Y, et al. Hierarchical network enabled flexible textile pressure sensor with ultrabroad response range and high-temperature resistance. Adv Sci, 2022, 9, 2105738
[12] Chen M, Wang Z X, Ge X, et al. Controlled fragmentation of single-atom-thick polycrystalline graphene. Matter, 2020, 2, 666
[13] Yuk H, Lu B, Zhao X, et al. Hydrogel bioelectronics. Chem Soc Rev, 2019, 48, 1642
[14] Lei Z Y, Wang Q K, Sun S, et al. A bioinspired mineral hydrogel as a self-healable, mechanically adaptable ionic skin for highly sensitive pressure sensing. Adv Mater, 2017, 29, 1700321
[15] Zhang H, Han W, Xu K, et al. Metallic sandwiched-aerogel hybrids enabling flexible and stretchable intelligent sensor. Nano Lett, 2020, 20, 3449
[16] Ma Z, Kong D S, Pan L J, et al. Skin-inspired electronics: emerging semiconductor devices and systems. J Semicond, 2020, 41, 041601
[17] Kim Y, Liu M J, Ishida Y, et al. Thermoresponsive actuation enabled by permittivity switching in an electrostatically anisotropic hydrogel. Nat Mater, 2015, 14, 1002
[18] Fukushima T, Asaka K, Kosaka A, et al. Fully plastic actuator through layer-by-layer casting with ionic-liquid-based bucky gel. Angew Chem Int Ed, 2005, 44, 2410
[19] He Y, Sun J, Qian C, et al. Solution-processed natural gelatin was used as a gate dielectric for the fabrication of oxide field-effect transistors. Org Electron, 2016, 38, 357
[20] Lu Y, Qu X, Zhao W, et al. Highly stretchable, elastic, and sensitive mxene-based hydrogel for flexible strain and pressure sensors. Research, 2020, 2020, 2038560
[21] Yang J, Yu X, Sun X, et al. Polyaniline-decorated supramolecular hydrogel with tough, fatigue-resistant, and self-healable perform-

ances for all-in-one flexible supercapacitors. ACS Appl Mater Interfaces, 2020, 12, 9736
[22] Cheng H, He X, Fan Z, et al. Flexible quasi-solid state ionogels with remarkable seebeck coefficient and high thermoelectric properties. Adv Energy Mater, 2019, 9, 1901085
[23] Shen Z, Zhu X, Majidi C, et al. Cutaneous ionogel mechanoreceptors for soft machines, physiological sensing, and amputee prostheses. Adv Mater, 2021, 33, 2102069
[24] Kwon J, Kim Y, Moon H, et al. Porous ion gel: A versatile ionotronic sensory platform for high-performance, wearable ionoskins with electrical and optical dual output. ACS Nano, 2021, 15, 15132
[25] Wang Y, Huang J. Recent advancements in flexible humidity sensors. J Semicond, 2020, 41, 040401
[26] Ma Y, Zhang Y, Cai S, et al. Flexible hybrid electronics for digital healthcare. Adv Mater, 2020, 32, 1902062
[27] Ma X H, Jiang Z F, Lin Y J. Flexible energy storage devices for wearable bioelectronics. J Semicond, 2021, 42, 101602
[28] Li C, Li P, Yang S, et al. Recently advances in flexible zinc ion batteries. J Semicond, 2021, 42, 101603
[29] Zhang Z, Chen C, Fei T, et al. Wireless communication and wireless power transfer system for implantable medical device. J Semicond, 2020, 41, 102403
[30] Zhao S F, Ran W H, Wang L L, et al. Interlocked MXene/rGO aerogel with excellent mechanical stability for a health-monitoring device. J Semicond, 2022, 43, 082601
[31] Fang Y, Cheng H, He H, et al. Stretchable and transparent ionogels with high thermoelectric properties. Adv Funct Mater, 2020, 30, 2004699
[32] Xu L, Huang Z, Deng Z, et al. A transparent, highly stretchable, solvent-resistant, recyclable multifunctional ionogel with underwater self-healing and adhesion for reliable strain sensors. Adv Mater, 2021, 33, 2105306
[33] Cao Y, Tan Y, Li S, et al. Self-healing electronic skins for aquatic environments. Nat Electron, 2019, 2, 75
[34] Ren Y, Guo J, Liu Z, et al. Ionic liquid-based click-Ionogels. Sci Adv, 2019, 5, eaax0648
[35] Cao Y, Morrissey T, Acome E, et al. A transparent, self-healing, highly stretchable ionic conductor. Adv Mater, 2017, 29, 1605099
[36] Li T, Wang Y, Li S, et al. Mechanically robust, elastic, and healable ionogels for highly sensitive ultra-durable ionic skins. Adv Mater, 2020, 32, 2002706
[37] Keum K, Eom J, Lee J, et al. Fully-integrated wearable pressure sensor array enabled by highly sensitive textile-based capacitive ionotronic devices. Nano Energy, 2021, 79, 105479
[38] Chen M, Luo W, Xu Z, et al. An ultrahigh resolution pressure sensor based on percolative metal nanoparticle arrays. Nat Commun, 2019, 10, 4024
[39] Shi L, Li Z, Chen M, et al. Quantum effect-based flexible and transparent pressure sensors with ultrahigh sensitivity and sensing density. Nat Commun, 2020, 11, 3529
[40] Gong S. Schwalb W, Wang Y, et al. A wearable and highly sensitive pressure sensor with ultrathin gold nanowires. Nat Commun, 2014, 5, 3132
[41] Mannsfeld S, Tee B C K, Stoltenberg R M, et al. Highly sensitive flexible pressure sensors with microstructured rubber dielectric layers. Nat Mater, 2010, 9, 859
[42] Burnworth M, Tang L, Kumpfer J, et al. Optically healable supramolecular polymers. Nature, 2011, 472, 334
[43] Meis CM, Grosskopf AK, Correa S, et al. Injectable supramolecular polymer-nanoparticle hydrogels for cell and drug delivery applications. J Vis Exp, 2021, 168, e62234
[44] Appel E, Tibbitt M, Webber M, et al. Self-assembled hydrogels utilizing polymer-nanoparticle interactions. Nat Commun, 2015, 6, 6295

Ruiyang Yin received his master's degree from the Institute of Semiconductors, Chinese Academy of Sciences. Now, he is a Ph.D. student at the School of Materials Science and Engineering, Peking University, and his research direction is the wearable sensing performance and preparation of large-area perovskite solar cells.

Linlin Li is currently a Ph.D. candidate at Institute of Semiconductors, Chinese Academy of Sciences. His current scientific interests focus on Te semiconductor materials-based multimodal integrated system.

Lili Wang is a professor in the Institute of Semiconductors, Chinese Academy of Sciences, China. She earned her B.S. (2010) degree in Chemistry and Ph.D. degree in Microelectronics and Solid State Electronics from Jilin University in 2014. Her current research interests focus on semiconductor materials-based multimodal sensing integrated systems for Human-Cyber-Physical Systems.

Zheng Lou is a professor in the Institute of Semiconductors, Chinese Academy of Sciences. He received his B.S. degree (2009) and his Ph.D. degree (2014) from Jilin University. His current research focuses on semiconductor photodetectors.